

Dynamic Adaptive and Adversarial Graph Convolutional Network for Traffic Forecasting

Juyong Jiang^{1*}, Binqing Wu^{2*}, Ling Chen^{2†}, Sunghun Kim¹

¹The Hong Kong University of Science and Technology

²Zhejiang University

{juyongjiang, hunkim}@ust.hk, {binqingwu, lingchen}@cs.zju.edu.cn

Abstract

Traffic forecasting is challenging due to dynamic and complicated spatial-temporal dependencies. However, existing methods still suffer from two critical limitations. Firstly, many approaches typically utilize static pre-defined or adaptively learned spatial graphs to capture dynamic spatial-temporal dependencies in the traffic system, which limits the flexibility and only captures shared patterns for the whole time, thus leading to sub-optimal performance. In addition, most approaches individually and independently consider the absolute error between ground truth and predictions at each time step, which fails to maintain the global properties and statistics of time series as a whole and results in trend discrepancy between ground truth and predictions. To this end, in this paper, we propose a Dynamic Adaptive and Adversarial Graph Convolutional Network (DAAGCN), which combines Graph Convolution Networks (GCNs) with Generative Adversarial Networks (GANs) for traffic forecasting. Specifically, DAAGCN leverages a universal paradigm with a gate module to integrate time-varying embeddings with node embeddings to generate dynamic adaptive graphs for inferring spatial-temporal dependencies at each time step. Then, two discriminators are designed to maintain the consistency of the global properties and statistics of predicted time series with ground truth at the sequence and graph levels. Extensive experiments on four benchmark datasets manifest that DAAGCN outperforms the state-of-the-art by average **5.05%**, **3.80%**, and **5.27%**, in terms of MAE, RMSE, and MAPE, meanwhile, speeds up convergence up to **9** times.¹

Introduction

With the continued development of urbanization, the city’s transportation infrastructure is under tremendous strain due to fast-increasing populations and cars. This circumstance calls for a more efficient intelligent transportation system (ITS) to increase traffic efficiency, improve public safety, and help make better city planning (Jiang et al. 2021; Jiang and Luo 2021; Li et al. 2021). As one of the essential parts of the ITS, traffic forecasting has become a research focus both in academic and industrial communities (Yu, Yin, and Zhu 2018).

*Equal Contribution.

†Corresponding Author.

Preprint. Under Review.

¹Code is available at <https://github.com/juyongjiang/DAAGCN>

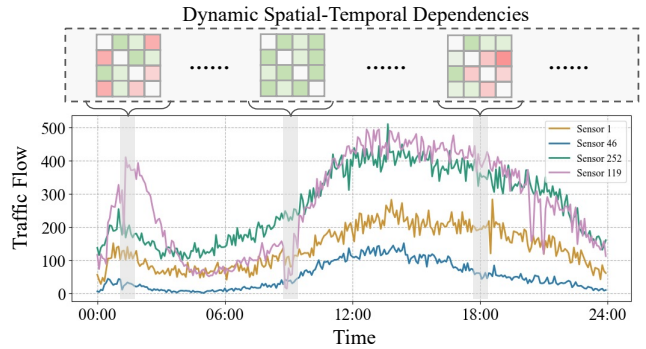


Figure 1: Examples of traffic flow observed by 4 sensors of PEMS04 dataset with dynamic spatial-temporal dependencies. Sensor 46, 252, and 119 are the adjacent sensors at geographic distance of Sensor 1.

Traffic forecasting aims to predict future traffic flow given historical observational data (Li et al. 2018). It is highly challenging due to dynamic and complicated spatial-temporal dependencies among traffic flow data, as shown in Fig. 1. Many approaches have been proposed for traffic forecasting in past decades, continuously improving from shallow machine learning (Makridakis and Hibon 1997; Wu, Ho, and Lee 2004) to deep learning (SHI et al. 2015; Li et al. 2018). Recently, spatial-temporal graph neural networks (STGNNs), a group of approaches integrating GNNs to model spatial dependencies with RNNs, CNNs, or Attentions to model temporal dependencies, have shown the state-of-the-art performance for traffic forecasting.

Despite this, most current STGNNs still suffer from two critical limitations. The first one is lacking the ability to model dynamic spatial dependencies among nodes. As illustrated in Fig. 1, the dependencies between nodes change as time progresses. However, existing STGNNs mainly depend on static pre-defined (Yu, Yin, and Zhu 2018; Geng et al. 2019; Guo et al. 2021) or adaptive (Wu et al. 2019; Bai et al. 2020; Chen et al. 2022b) adjacency matrices (spatial graphs). These static adjacency matrices cannot reflect dynamic spatial dependencies, which leads to sub-optimal spatial-temporal dependencies modeling and further limits the effectiveness and practicability of STGNNs in real-world applications.

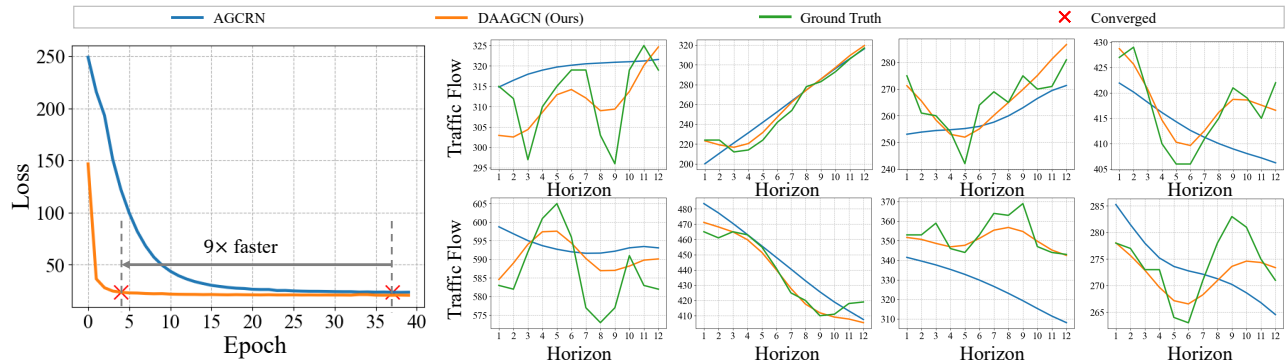


Figure 2: Convergence and predicted results of DAAGCN on PEMS07 dataset. The left sub-figure shows that DAAGCN converges 9 times faster than AGCRN and yields lower training loss. The right eight sub-figures, corresponding to randomly selected eight nodes, show the predicted traffic flow at each horizon. It can be observed that the predicted results of DAAGCN are closer to ground truth and have a more similar global trend to ground truth. More results are presented in Appendix C.1.

What’s more, another limitation is that current traffic forecasting approaches fail to maintain the global properties and statistics of time series as a whole (e.g., the overall trend and correlations of time series between all nodes), resulting in trend discrepancy between ground truth and predictions (see green and blue curves in the right side of Fig. 2). The reason behind this is that most existing traffic forecasting approaches optimize their networks by absolute differences between true and predicted point values within fixed horizon steps. In fact, this optimizing strategy only justifies the predicted point values individually and independently, which neglects that the global properties and statistics among ground truth and predicted time series should also be consistent, thus leading to sub-optimal performance.

To tackle these limitations, we propose a Dynamic Adaptive and Adversarial Graph Convolutional Network (DAAGCN) under Generative Adversarial Networks (GANs) framework for traffic forecasting, which not only models dynamic spatial dependencies but also maintains the consistency of the global properties and statistics of predicted time series with ground truth at the sequence and graph levels. The main contributions of our work are summarized as follows:

- Inspired by the success of GCNs and GANs, this work attempts to combine GCNs with GANs for traffic forecasting. It encapsulates the advantages of GCNs and GANs, and shows great potential for time series forecasting, e.g., faster convergence and better predicted results (see Fig. 2).
- We propose a dynamic adaptive graph generation (DAGG) module that leverages a universal paradigm with a gate module to integrate time-varying embeddings with node embeddings, which can model the dynamic spatial dependencies and eliminate the reliance on prior or domain knowledge.
- We introduce two discriminators that discriminate whether the global properties and statistics of predicted time series aligned with ground truth at the sequence and graph levels, which bridges the trend discrepancy be-

tween predictions and ground truth.

- We evaluate the proposed model on four traffic benchmark datasets. Extensive experiments demonstrate that DAAGCN outperforms the state-of-the-art methods by average **5.05%** relative MAE reduction, **3.80%** relative RMSE reduction, and **5.27%** relative MAPE reduction, meanwhile, speeds up convergence up to **9** times.

Related Work

Traffic Forecasting

As a critical component of ITS, traffic forecasting has been studied for decades. Early traffic forecasting approaches, e.g., ARIMA (Makridakis and Hibon 1997), VAR (Zivot and Wang 2006), and SVR (Wu, Ho, and Lee 2004), mainly concentrate on the temporal dependencies of a node itself or shared by a few nodes, which barely captures the spatial dependencies among nodes. Encouraged by the development of deep learning technologies, recurrent neural networks (RNNs), convolution neural networks (CNNs), and their hybrid models (Ma et al. 2017; Yu et al. 2017; Zhang et al. 2018) are applied to capture nodes’ temporal dependencies and regular spatial dependencies effectively. In contrast, non-Euclidean spatial dependencies dominated by existing irregular road networks are not considered.

Recently, Graph neural networks (GNNs) have shown their superior ability to model non-Euclidean spatial dependencies among nodes (Wu et al. 2021). In particular, a group of GNNs, known as spatial-temporal graph neural networks (STGNNs), has shown the state-of-the-art performance for traffic flow forecasting. These STGNNs integrate GNNs to model spatial dependencies with RNNs (Li et al. 2018; Chen et al. 2020), CNNs (Yu, Yin, and Zhu 2018; Geng et al. 2019), or Attention (Guo et al. 2019; Zheng et al. 2020; Guo et al. 2021) to model temporal dependencies. However, the performance of these STGNNs is highly dependent on static pre-defined adjacency matrices obtained from prior or domain knowledge. Although there are some recent approaches that have tried to learn adjacency matrices from data by using learnable node embeddings (Wu et al. 2019;

Bai et al. 2020) or hidden representations of node features (Cao et al. 2020), their performance is still restrained by the ability to model dynamic spatial dependencies. Therefore, in our work, we propose a DAGG module, which can learn dynamic spatial dependencies with good interpretability from data automatically.

Generative Adversarial Networks for Times Seires

Generative Adversarial Networks (GANs) are generative models that learn to produce realistic data adversarially. They have achieved remarkable success in computer vision and natural language processing, and have also shown promising performance for time series applications. TimeGAN (Yoon, Jarrett, and van der Schaar 2019) first introduces GANs to time series generation. It utilizes GANs based on a learned embedding space to generate time series data that preserve temporal dynamics. AST (Wu et al. 2020) promotes GANs for time series forecasting. It adopts a Sparse Transformer as the generator to learn a sparse attention map, and uses a discriminator to eliminate the error accumulation at the sequence level. TrafficGAN (Zhang et al. 2021) utilizes GANs for traffic forecasting. It utilizes CNN and LSTM to capture the spatial-temporal dependencies, with adversarial training to learn the distribution of the future traffic flows. More recently, PSA-GAN (Jeha et al. 2022) generates long time series samples using progressive growing of GANs and self-attention for several downstream time series forecasting tasks. However, these works barely explicitly consider the global properties and statistics (e.g., the overall trend and correlations of time series between all nodes) when generating or discriminating samples.

Preliminaries

Problem Definition

In this paper, we aim to solve multi-step traffic forecasting problem, given observed historical time series. Formally, define these time series as a set $\mathbf{X}^{1:T} = \{\mathbf{x}^1, \mathbf{x}^2, \dots, \mathbf{x}^t, \dots, \mathbf{x}^T\} \in \mathbb{R}^{T \times N \times C}$, where $\mathbf{x}^t \in \mathbb{R}^{N \times C}$ denotes observed values with C feature dimensions of N nodes at time step t , and x_i^t represents the value of the i -th node at time step t . Our target is to find a mapping function \mathcal{F} to forecast the next H steps data based on the past T steps data. Thus, the traffic forecasting problem can be formulated as:

$$\hat{\mathbf{X}}^{T+1:T+H} = \mathcal{F}(\mathbf{X}^{1:T}; \Theta) \quad (1)$$

where $\hat{\mathbf{X}}^{T+1:T+H} \in \mathbb{R}^{H \times N \times F}$, H denotes the forecasting horizon and F is the output feature dimensions of each node. \mathcal{F} is the mapping function, and Θ denotes all learnable parameters in the model.

Graph Convolution

Graph convolution networks (GCNs) have drawn considerable attention to accurately capturing spatial dependencies between different time series with non-Euclidean structures, i.e., graph. Therefore, in our work, we employ GCNs (Wu et al. 2021; Chen et al. 2020; Bai et al. 2020) to capture spatial dependencies for traffic forecasting problem at each time

step t . Specifically, given a graph $\mathcal{G} = (\mathbf{V}, \mathbf{E}, \mathbf{A})$, where \mathbf{V} denotes a set of $|\mathbf{V}| = N$ nodes, \mathbf{E} is a set of edges, and \mathbf{A} represents adjacency matrix. Thus, the above problem can be further formulated as:

$$\mathbf{Z} = \mathcal{G}(\mathbf{X}^{(t)}; \Theta) = \sigma(\tilde{\mathbf{D}}^{-1} \tilde{\mathbf{A}} \mathbf{X}^{(t)} \Theta) \quad (2)$$

where $\tilde{\mathbf{A}} = \mathbf{I}_N + \mathbf{A}$ and $\tilde{\mathbf{D}}^{-1}$ are the adjacency matrix of the graph with self-connection and its corresponding diagonal degree matrix, respectively. Thus, the normalized adjacency matrix can be denoted by $\tilde{\mathbf{D}}^{-1} \tilde{\mathbf{A}}$. $\mathbf{X}^{(t)} = \mathbf{x}^t \in \mathbb{R}^{N \times C}$ and $\mathbf{Z} \in \mathbb{R}^{N \times F}$ are the input and output of the GCNs, respectively. $\Theta \in \mathbb{R}^{C \times F}$ denotes the learnable parameters of the model. $\sigma(\cdot)$ is an activation function.

Methodology

Model Overview

DAAGCN consists of (1) dynamic adaptive graph generation (DAGG) for capturing dynamic spatial dependencies from data automatically; and (2) graph convolutional RNN with adversarial training (AGC-GRU) for modeling temporal correlations and maintaining the global properties and statistics of time series aligned with ground truth. The overall model architecture is shown in Fig. 3.

Dynamic Adaptive Graph Generation

For GCN-based traffic forecasting models, one critical problem is how to precisely model complex spatial dependencies between different spatial nodes, i.e., adjacency matrix \mathbf{A} , for the graph convolution operation. To define \mathbf{A} , existing works can be roughly divided into three main categories: (1) distance function (Li et al. 2018; Yu, Yin, and Zhu 2018), which leverages geographic (spatial) distance between different nodes; (2) similarity function (Bai et al. 2019b; Geng et al. 2019; Bai et al. 2019a), which measure the similarity of node attributes; (3) adaptive function (Bai et al. 2020; Wu et al. 2019; Chen et al. 2022a), which infer spatial dependencies by learnable node embeddings. In particular, the third category, i.e., adaptive function, has been a prevalent method to define graphs, as it can learn spatial dependencies from data automatically without the guidance of prior or domain knowledge.

However, above mentioned approaches of graph generation neglect the fact that the spatial-temporal dependencies are dynamic over time (see Fig. 1). To this end, we propose a Dynamic Addaptive Graph Generation (DAGG) module to capture dynamic spatial dependencies from data automatically. Our DAGG module first randomly initializes a learnable node embeddings $\mathbf{E}_{\text{node}} \in \mathbb{R}^{N \times d_1}$ for all nodes (Bai et al. 2020; Wu et al. 2019; Chen et al. 2022a), where each row of \mathbf{E}_{node} denotes the embedding of each node and d_1 is the hidden dimension of node embeddings. Then, we explicitly introduce time-varying information through learnable time-varying embeddings $\mathbf{E}_{\text{time}} \in \mathbb{R}^{T \times d_2}$, where each row of \mathbf{E}_{time} represents the embedding of each time step t and d_2 is the hidden dimension of time-varying embeddings. To keep the consistency of dimension in the following operations, we set $d = d_1 = d_2$ by default. However, it is still an

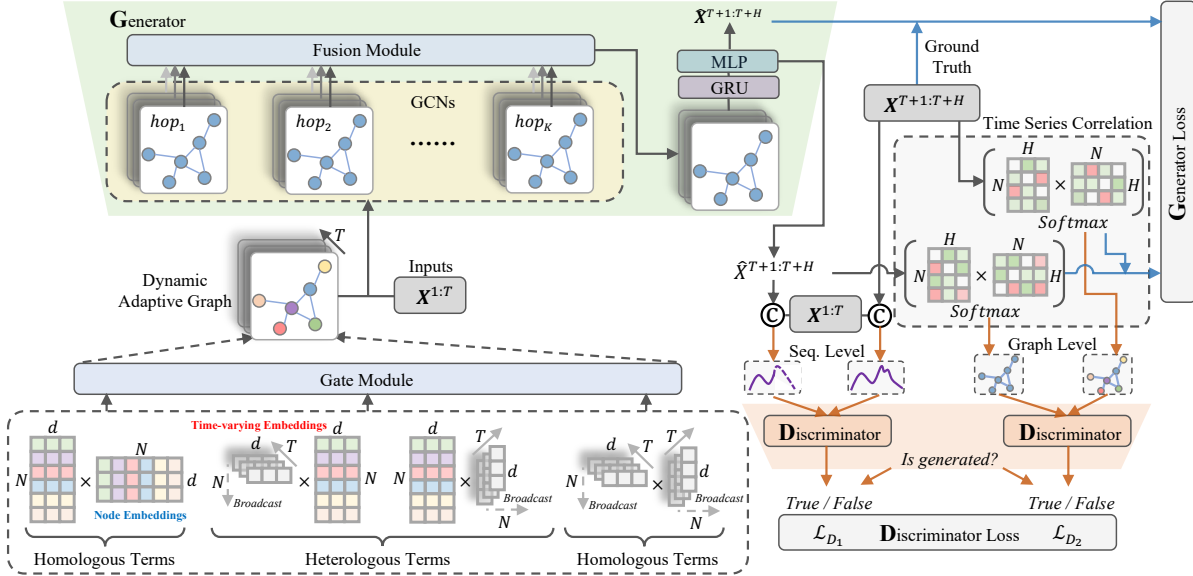


Figure 3: The model architecture of the proposed DAAGCN.

open challenge about how to effectively combine node embeddings with time-varying embeddings, as heterogeneous information may restrict or exclude each other (Vaswani et al. 2017; Shaw, Uszkoreit, and Vaswani 2018; Dai et al. 2019; Jiang, Zhang, and Zhang 2020; Raffel et al. 2020). To address this challenge, we propose a universal paradigm to integrate time-varying embeddings with node embeddings and adaptively assigns different important weights through a gate module to trade off the interaction between different information terms. Let E_{node}^i and E_{time}^t be the i th node embedding and time-varying embedding at time step t . Then, dynamic spatial dependencies between each pair of i th and j th node are computed as:

$$A_{ij} = \lambda \{ E_{\text{node}}^i \Delta_1 E_{\text{time}}^t, E_{\text{node}}^j \Delta_2 E_{\text{time}}^t \} \quad (3)$$

where $\Delta_1, \Delta_2 \in \{+, \odot, \parallel\}$, \odot and \parallel represent hadamard product and concatenation operation, respectively, $\{\cdot, \cdot\}$ denotes the inner product, and λ represents the important weights of each kind of information terms. In particular, when $\Delta_1 = +, \Delta_2 = +$, Eq. 3 can be expanded as:

$$\begin{aligned} A_{ij} &= \lambda \{ E_{\text{node}}^i + E_{\text{time}}^t, E_{\text{node}}^j + E_{\text{time}}^t \} \\ &= \lambda_1 \underbrace{\{ E_{\text{node}}^i, E_{\text{node}}^j \}}_{\text{homologous terms}} + \lambda_2 \underbrace{\{ E_{\text{node}}^i, E_{\text{time}}^t \} + \{ E_{\text{node}}^j, E_{\text{time}}^t \}}_{\text{heterologous terms}} \\ &\quad + \lambda_3 \underbrace{\{ E_{\text{time}}^t, E_{\text{time}}^t \}}_{\text{homologous terms}} \end{aligned} \quad (4)$$

The cases of multiplication ($\Delta_1 = \odot, \Delta_2 = \odot$), concatenation ($\Delta_1 = \parallel, \Delta_2 = \parallel$), and hybrid ($\Delta_1 = +, \Delta_2 = \odot$) fusion are discussed in Appendix C.4, due to space limit. Finally, following previous works (Bai et al. 2020; Wu et al. 2019; Chen et al. 2022a), we employ 1^{st} order Chebyshev polynomial expansion to approximate graph convolution operation with node-aware parameters, then the DAGG module

can be formulated as:

$$Z = (I_N + \text{softmax}(A)) X E_{\text{node}} W + E_{\text{node}} b \quad (5)$$

where $W \in R^{d \times C \times F}$, $b \in R^{d \times F}$, and softmax function is leveraged to normalize the adaptive matrix A . During training, E_{node} and E_{time} are updated to learn dynamic spatial-temporal dependencies between different nodes at each time step for graph convolution operation. In addition, it is worth noting that we do not adopt any activation function before softmax normalization. More in-depth discussions are presented in Appendix C.5.

Adversarial Graph Convolutional RNN

RNNs as a simple but effective model have shown great success in capturing temporal correlations. Following prior works (Chen et al. 2020; Bai et al. 2020), we integrate proposed DAGG module to Gated Recurrent Units (GRU) (Chung et al. 2014) by replacing the MLP layers in GRU. Then, we stack several GRU layers followed by a linear transformation (MLP) to project the output of GRU to achieve multi-step ahead traffic forecasting in the manner of sequence to sequence, which significantly decreases the cost of time. Formally, it can be formulated as:

$$\begin{aligned} z^{(t)} &= \sigma(\mathcal{G}([X^{(t)}, h^{(t-1)}]; \Theta_z)) \\ r^{(t)} &= \sigma(\mathcal{G}([X^{(t)}, h^{(t-1)}]; \Theta_r)) \\ c^t &= \tanh(\mathcal{G}([X^{(t)}, r^{(t)} \odot h^{(t-1)}]; \Theta_c)) \\ h^{(t)} &= z^{(t)} \odot h^{(t-1)} + (1 - z^{(t)}) \odot c^t \\ \hat{X}^{T+1:T+H} &= h^{(T)} W + b \end{aligned} \quad (6)$$

where $X^{(t)}$ and $h^{(t)}$ represent input and output at time step t , $[\cdot, \cdot]$ denotes the concatenation operation, $z^{(t)}$ and $r^{(t)}$ denote reset gate and update gate at time step t , respectively.

\mathcal{G} represents DAGG module with learnable parameters Θ_z , Θ_r , and Θ_c . W and b are learnable parameters in linear transformation (MLP).

Adversarial Training The downside of the above generative approach is that the global properties and statistics of traffic series are ignored, as predictions are made individually and independently at each time step.

To solve this problem, we introduce adversarial training to discriminate whether the predicted H horizon time series have the same global properties and statistics as ground truth at the sequence and graph levels. We refer this special RNN module as Adversarial Graph Convolutional GRU (AGC-GRU), as shown in Fig. 3. Furthermore, we combine DAGG with AGC-GRU as a generator network \mathcal{G} and introduce two discriminators to align with ground truth at the sequence level (D_1) and the graph level (D_2), which both consist of three fully connected linear layers (Makhzani et al. 2016; Wu et al. 2020) with *LeakReLU*.

Note that, the sequence level focuses on the trend of traffic series, and the graph level emphasizes the correlation of traffic series between all nodes. Both are very important for traffic forecasting.

Formally, the loss functions of minmax optimization problem are formulated as:

$$\begin{aligned}\mathcal{L}_{D_1} &= -\mathbb{E}_{x_r^1 \sim \mathbb{P}} [\log(D_1(x_r^1))] - \mathbb{E}_{x_f^1 \sim \mathbb{Q}} [\log(1 - D_1(x_f^1))] \\ \mathcal{L}_{D_2} &= -\mathbb{E}_{x_r^2 \sim \mathbb{P}} [\log(D_2(x_r^2))] - \mathbb{E}_{x_f^2 \sim \mathbb{Q}} [\log(1 - D_2(x_f^2))] \\ \mathcal{L}_G &= \alpha(-\mathbb{E}_{x_r^1 \sim \mathbb{P}} [\log(1 - D_1(x_r^1))] - \mathbb{E}_{x_f^1 \sim \mathbb{Q}} [\log(D_1(x_f^1))] \\ &\quad) + \beta(-\mathbb{E}_{x_r^2 \sim \mathbb{P}} [\log(1 - D_2(x_r^2))] - \mathbb{E}_{x_f^2 \sim \mathbb{Q}} [\log(D_2(x_f^2))])\end{aligned}\quad (7)$$

where

$$\begin{aligned}\text{Sequence Level : } &\begin{cases} x_r^1 = (\mathbf{X}^{1:T} \parallel \mathbf{X}^{T+1:T+H}) \\ x_f^1 = (\mathbf{X}^{1:T} \parallel \hat{\mathbf{X}}^{T+1:T+H}) \end{cases} \\ \text{Graph Level : } &\begin{cases} x_r^2 = \delta((\mathbf{X}^{T+1:T+H})^\top \mathbf{X}^{T+1:T+H}) \\ x_f^2 = \delta((\hat{\mathbf{X}}^{T+1:T+H})^\top \hat{\mathbf{X}}^{T+1:T+H}) \end{cases}\end{aligned}\quad (8)$$

Here, x_r^1 and x_r^2 denote the ground truth (real) sampled from distribution \mathbb{P} , x_f^1 and x_f^2 is the predicted (fake) time series sampled from distribution \mathbb{Q} . \mathcal{T} and \parallel denote the transpose and concatenation operations, respectively, $\delta(\cdot)$ is *softmax* normalization. α and β represent the trade-off weights to balance \mathcal{L}_{D_1} and \mathcal{L}_{D_2} .

Overall Loss We utilize L1 loss as training objective and jointly optimize the loss with the adversarial training loss for the generator to make multi-step predictions. Thus, the overall loss of our DAAGCN is formulated as:

$$\mathcal{L} = \mathcal{L}_p(\Theta) + \mathcal{L}_G, \mathcal{L}_p(\Theta) = \sum_{t=T+1}^{T+H} |\mathbf{X}^{(t)} - \hat{\mathbf{X}}^{(t)}| \quad (9)$$

where $\mathbf{X}^{(t)}$ and $\hat{\mathbf{X}}^{(t)}$ denote ground truth and predicted results of all nodes at time step i , Θ is all the learnable parameters in the generator. The overall training algorithm is described in Algorithm 1.

Algorithm 1: Adversarial Training for DAAGCN

Input : Training data \mathbf{X} , maximum epoch E , learning rate η_1 for model (generator), learning rate η_2 for two discriminators.

Output: The generator parameters Θ .

Initialize the generator parameters Θ and two discriminators parameters θ_1 and θ_2 .

for $e = 1$ to E **do**

Randomly sample $[\mathbf{X}^{1:T}, \mathbf{X}^{T+1:T+H}]$ from \mathbf{X} ;
 Generate dynamic adaptive graph with node embeddings \mathbf{E}_{node} and time-varying embeddings \mathbf{E}_{time} by Eq. 3;
 Capture dynamic spatial dependencies between all nodes with the DAGG module by Eq. 5;
 Capture temporal correlations and generate multi-step predictions $\hat{\mathbf{X}}^{T+1:T+H}$ with the AGC-GRU module by Eq. 6;
 Construct the ground truth (real) samples and predicted (fake) time series samples from the sequence level (x_r^1 and x_f^1) and the graph level (x_r^2 and x_f^2) by Eq. 8.
 Calculate two discriminators loss \mathcal{L}_{D_1} and \mathcal{L}_{D_2} by Eq. 7;
 Calculate the generator loss \mathcal{L}_G by Eq. 7;
 Calculate the total training loss \mathcal{L} by Eq. 9;
 Update the generator parameters by minimizing loss \mathcal{L} :
 $\Theta \leftarrow \Theta - \eta_1 \frac{\partial \mathcal{L}}{\partial \Theta}$;
 Update two discriminators parameters by minimizing loss \mathcal{L}_{D_1} and \mathcal{L}_{D_2} :
 $\theta_1 \leftarrow \theta_1 - \eta_2 \frac{\partial \mathcal{L}_{D_1}}{\partial \theta_1}, \theta_2 \leftarrow \theta_2 - \eta_2 \frac{\partial \mathcal{L}_{D_2}}{\partial \theta_2}$.

end

return The generator parameters Θ .

Experiments

Dataset

To evaluate the proposed DAAGCN, we conduct extensive empirical studies with four real-world traffic benchmark datasets, including PEMS03, PEMS04, PEMS07, and PEMS08, which are collected from the Caltrans Performance Measurement System (PeMS) (Guo et al. 2019; Song et al. 2020). We follow the common data preprocessing procedure (Li and Zhu 2021; Bai et al. 2020; Chen et al. 2020) to fill the missing data by linear interpolation, then aggregate data into 5-minute time interval. In addition, we normalize all datasets using the Z-Score normalization method. The detailed dataset statistics are summarized in Table 2.

Baselines

We compare DAAGCN both with temporal models that do not require a pre-defined graph and spatial-temporal models that rely on a pre-defined or adaptively learned graph.

- The following temporal models are considered: Vector Auto-Regression (VAR) (Zivot and Wang 2006); Auto-Regressive Integrated Moving Average (ARIMA) (Makridakis and Hibon 1997); FC-LSTM (SHI et al. 2015), using fully connected LSTMs to capture the non-linear temporal dependencies; TCN (Bai, Kolter, and Koltun 2018), consisting of a stack of causal convolutional layers with exponentially enlarged dilation factors for sequence modeling tasks.
- The following spatial-temporal models are included: DCRNN (Li et al. 2018), integrating diffusion convolution with sequence-to-sequence architecture; STGCN

Table 1: Prediction performance comparison of different models on four datasets. Bold scores are the best in each column, while underlined scores are the second best. a , b , and c denote adaptive graph based methods.

Model	PEMS03			PEMS04			PEMS07			PEMS08		
	MAE	RMSE	MAPE(%)	MAE	RMSE	MAPE(%)	MAE	RMSE	MAPE(%)	MAE	RMSE	MAPE(%)
ARIMA	35.41	47.59	33.78	33.73	48.80	24.18	38.17	59.27	19.46	31.09	44.32	22.73
VAR	23.65	38.26	24.51	24.52	38.61	17.24	50.22	75.63	32.22	19.19	29.81	13.10
FC-LSTM (NIPS 2015)	21.33	35.11	23.33	26.77	40.65	18.23	29.98	45.94	13.20	23.09	35.17	14.99
TCN (ICLR 2018)	19.32	33.55	19.93	23.22	37.26	15.59	32.72	42.23	14.26	22.72	35.79	14.03
DCRNN (ICLR 2018)	17.99	30.31	18.34	21.22	33.44	14.17	25.22	38.61	11.82	16.82	26.36	10.92
STGCN (IJCAI 2018)	17.55	30.42	17.34	21.16	34.89	13.83	25.33	39.34	11.21	17.50	27.09	11.29
ASTGCN (AAAI 2019)	17.34	29.56	17.21	22.93	35.22	16.56	24.01	37.87	10.73	18.25	28.06	11.64
^a GraphWaveNet (IJCAI 2019)	19.12	32.77	18.89	24.89	39.66	17.29	26.39	41.50	11.97	18.28	30.05	12.15
STSGCN (AAAI 2020)	17.48	29.21	16.78	21.19	33.65	13.90	24.26	39.03	10.21	17.13	26.80	10.96
STFGNN (AAAI 2021)	16.77	28.34	16.30	19.83	31.88	13.02	22.07	35.80	<u>9.21</u>	16.64	26.22	10.60
^b AGCRN (NIPS 2020)	<u>16.03</u>	28.52	<u>14.65</u>	19.89	32.86	13.37	22.37	35.70	9.55	16.13	25.52	10.21
^c Z-GCNETs (ICML 2021)	16.64	<u>28.15</u>	16.39	19.50	<u>31.61</u>	<u>12.78</u>	<u>21.77</u>	<u>35.17</u>	9.25	<u>15.76</u>	<u>25.11</u>	<u>10.01</u>
DAAGCN (ours)	14.77	25.66	13.92	18.81	30.68	12.25	20.70	35.16	8.57	15.15	24.26	9.51
Improvement	7.86%	8.85%	4.98%	3.54%	2.94%	4.15%	4.92%	0.03%	6.95%	3.87%	3.39%	5.00%

Table 2: Statistics of the four traffic benchmark datasets.

Dataset	PEMS03	PEMS04	PEMS07	PEMS08
# of nodes	358	307	883	170
# of timesteps	26,208	16,992	28,224	17,856
# Granularity	5min	5min	5min	5min
# Start time	9/1/2018	1/1/2018	5/1/2017	7/1/2016
# End time	11/30/2018	2/28/2018	8/31/2017	8/31/2016

(Yu, Yin, and Zhu 2018), merging graph convolution with gated temporal convolutions; ASTGCN (Guo et al. 2019), integrating attention mechanisms to capture dynamic spatial-temporal patterns; Graph WaveNet (Wu et al. 2019), combining graph convolution with dilated casual convolution; STSGCN (Song et al. 2020), utilizing localized spatial-temporal subgraph module to model localized correlations independently; STFGCN (Li and Zhu 2021), fusing various spatial and temporal graphs to handle long sequences; AGCRN, (Bai et al. 2020) using adaptive adjacency matrix for graph convolution and GRU to model temporal correlations; Z-GCNETs (Chen, Segovia, and Gel 2021), integrating the new time-aware zigzag topological layer into time-conditioned GCNs.

Experimental Settings

We split the dataset into three parts, including training sets, validation sets, and test sets with a ratio of 6:2:2 on PEMS03, PEMS04, PEMS07, and PEMS08 datasets. Then, we preprocess the datasets to generate 12 data points (time steps) per hour. At the training stage, we utilize the historical one hour data ($T = 12$) to forecast next hour data ($H = 12$). However, at the testing stage, only the present one hour data are utilized for predictions, following works (Bai et al. 2020; Chen et al. 2020; Yu, Yin, and Zhu 2018). For all baselines, some of the reported results are directly cited from existing works (Bai et al. 2020; Cao et al. 2020), while some of them are conducted by ourselves using authors provided source codes under each model’s own optimal hyper-parameter settings. Furthermore, three common metrics are leveraged to measure the performance of each model, including MAE, RMSE, and MAPE. We set $\alpha = 0.01$ and $\beta = 0.1$ in Eq. 7. More detailed settings are illustrated in Appendix A.

Performance Comparison and Analysis

The overall prediction performance is summarized in Table 1, where four temporal models and eight spatial-temporal models are compared, and each value represents the averaged MAE, RMSE, and MAPE over 12 prediction horizons. We can observe that: 1) DAAGCN outperforms the state-of-the-art by average **5.05%**, **3.80%**, and **5.27%**, in MAE, RMSE, and MAPE, which achieves a new state-of-the-art performance for traffic forecasting. 2) Compared with three adaptive graph based methods, i.e., GraphWaveNet, AGCRN, and Z-GCNETs, DAAGCN yields an average **11.36%** relative MAE reduction, **9.77%** relative RMSE reduction, and **13.97%** relative MAPE reduction over all datasets. It verifies that modeling dynamic adaptive graphs to capture dynamic spatial-temporal dependencies can significantly improve the prediction performance. The results of the ablation studies in Table 3 verify this as well. 3) The prediction performance at each horizon on PEMS04 dataset is shown in Fig. 4. We notice that DAAGCN achieves lower prediction errors on all metrics for all horizons by a large margin, indicating its strength in short term and long term forecasting. More results are provided in Appendix C.2.

Ablation Study

To explore the effect of each component in DAAGCN, we conduct ablation study with its variants, including with/without dynamic graph generation (DAGG) and adversarial graph training (AGC-GRU), as shown in Table 3. We observe that variants with dynamic graph consistently outperform variants with static graph. It again verifies that modeling dynamic adaptive graph is more effective and suitable for traffic forecasting. Moreover, introducing adversarial graph training at the sequence and graph levels can bring significant improvements to all variants, especially for variants with static graph. In addition, adversarial training at the graph level is better than at the sequence level. It implies that the correlation of traffic series between all nodes may contain more useful information about a traffic system. Overall, our proposed DAGG and AGC-GRU can be readily incorporated into other spatial-temporal models to benefit the prediction performance. Furthermore, we analyze the influence of different coefficient weights for the homologous term and

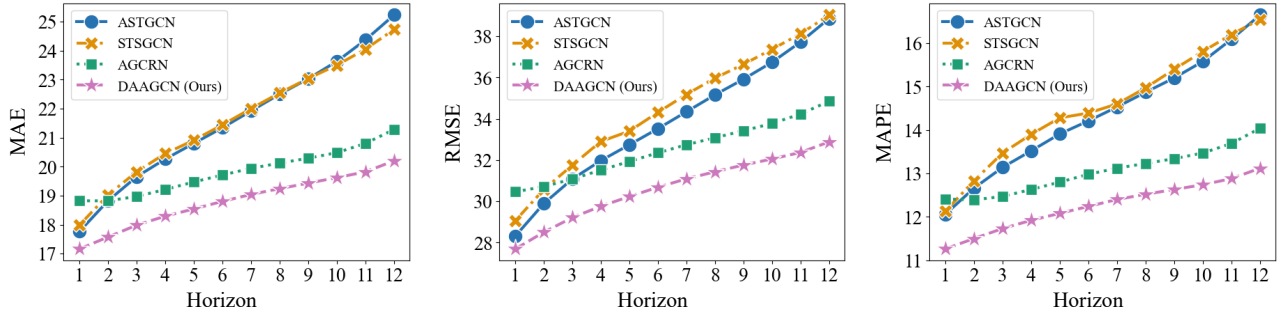


Figure 4: Prediction performance comparison at each horizon on PEMS04 dataset, in terms of MAE, RMSE, and MAPE.

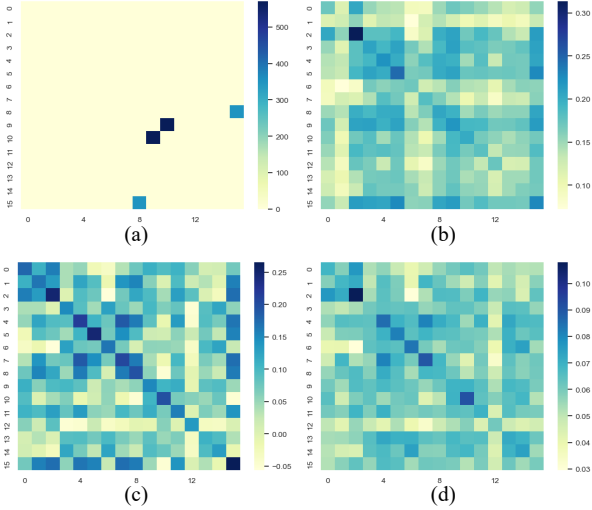


Figure 5: Visualization of dynamic adaptive graphs at different time steps. (a) distance adjacency matrix. (b) (c) (d) adaptively learned graph matrices at time step 1, 6, and 12.

heterologous term in DAGG when $\Delta_1 = +, \Delta_2 = +$ (see Eq. 4), as shown in Table 4. We notice that equally fusing them is the best choice. More detailed results are provided in Appendix C.3 and 4.

Visualization

In this section, we first randomly select 16 nodes, then visualize their static geographic distance matrix and our dynamic adaptive graph at the time step 1, 6, and 12 on PEMS04 dataset, aiming to discuss the interpretability of DAAGCN, as shown in Fig. 5. We derive the following observations: 1) Although many methods using pre-defined graphs have achieved comparable performance, they generally face the problem of data sparsity, as shown in Fig. 5(a), which harms the propagation of model’s gradient significantly. 2) Dynamic adaptive graphs can flexibly capture the spatial-temporal dependencies between all nodes at different time steps, as shown in Fig. 5 (b)(c)(d). More detailed results can be found in Appendix C.5. 3) The values on the diagonal of dynamic adaptive graphs are larger, which indicates that the self-connections play important role for traffic forecasting.

Table 3: Ablation study of our DAAGCN with different modules on PEMS04 dataset. Bold scores are the best in each column.

Settings			Results		
DYNAMIC	SEQ.	GRAPH	MAE	RMSE	MAPE(%)
✗	✗	✗	19.89	32.86	13.37
✗	✓	✗	19.43	32.19	12.77
✗	✗	✓	19.33	31.82	12.93
✓	✗	✗	19.00	31.54	12.36
✓	✓	✗	19.05	31.71	12.55
✓	✗	✓	18.97	31.79	12.38
✓	✓	✓	18.81	30.68	12.25

Table 4: Influence of different coefficient weights for the homologous term and heterologous term in DAGG on PEMS04 dataset. Bold scores are the best in each row.

Results	$\lambda = (\lambda_1, \lambda_2, \lambda_3)$					
	(1,0,0)	(1,1,0)	(0,1,1)	(1,0,1)	(0,1,0)	(1,1,1)
MAE	19.22	19.12	18.98	18.98	18.96	18.81
RMSE	32.12	31.92	31.66	31.71	31.53	30.68
MAPE(%)	12.48	12.46	12.51	12.50	12.32	12.25

Conclusions and Future Work

In this paper, we attempt to combine GCNs with GANs for traffic forecasting and propose Dynamic Adaptive and Adversarial Graph Convolutional Network, named DAAGCN. Specifically, to capture dynamic spatial-temporal dependencies in practical traffic systems, the dynamic adaptive graph generation (DAGG) is proposed. In addition, graph convolutional RNN with adversarial training (AGC-GRU) is proposed to model complex temporal correlations and maintain the global properties and statistics of traffic series aligned with ground truth, thereby bridging the trend discrepancy and correlations of time series between ground truth and predictions. DAAGCN achieves the state-of-the-art performance and enjoys up to 9 times faster model convergence on four traffic benchmark datasets. For further work, we will study the following two aspects: (1) investigating better methods to capture dynamic spatial-temporal dependencies, e.g., the mixture of experts (MoE); (2) exploring more effective approaches to maintain the global properties and statistics of traffic series aligned with ground truth, e.g., the change rate of time series.

References

- Bai, L.; Yao, L.; Kanhere, S. S.; Wang, X.; and Sheng, Q. Z. 2019a. STG2Seq: Spatial-temporal graph to sequence model for multi-step passenger demand forecasting. In *Proceedings of the International Joint Conference on Artificial Intelligence*, 1981–1987.
- Bai, L.; Yao, L.; Kanhere, S. S.; Yang, Z.; Chu, J.; and Wang, X. 2019b. Passenger demand forecasting with multi-task convolutional recurrent neural networks. In *Pacific-Asia Conference on Knowledge Discovery and Data Mining*, 29–42.
- Bai, L.; Yao, L.; Li, C.; Wang, X.; and Wang, C. 2020. Adaptive graph convolutional recurrent network for traffic forecasting. In *Advances in Neural Information Processing Systems*, 17804–17815.
- Bai, S.; Kolter, J. Z.; and Koltun, V. 2018. An empirical evaluation of generic convolutional and recurrent networks for sequence modeling. In *International Conference on Learning Representations Workshop*.
- Cao, D.; Wang, Y.; Duan, J.; Zhang, C.; Zhu, X.; Huang, C.; Tong, Y.; Xu, B.; Bai, J.; Tong, J.; and Zhang, Q. 2020. Spectral temporal graph neural network for multivariate time-series forecasting. In *Advances in Neural Information Processing Systems*, 17766–17778.
- Chen, L.; Chen, D.; Shang, Z.; Zhang, Y.; Wen, B.; and Yang, C. 2022a. Multi-scale adaptive graph neural network for multivariate time series forecasting. *arXiv*.
- Chen, W.; Chen, L.; Xie, Y.; Cao, W.; Gao, Y.; and Feng, X. 2020. Multi-range attentive bicomponent graph convolutional network for traffic forecasting. In *Proceedings of the AAAI Conference on Artificial Intelligence*, 3529–3536.
- Chen, Y.; Segovia, I.; and Gel, Y. R. 2021. Z-GCNETs: Time zigzags at graph convolutional networks for time series forecasting. In *International Conference on Machine Learning*, 1684–1694.
- Chen, Y.; Segovia-Dominguez, I.; Coskunuzer, B.; and Gel, Y. 2022b. TAMP-S2GCNETs: Coupling time-aware multipersistance knowledge representation with spatio-supra graph convolutional networks for time-series forecasting. In *International Conference on Learning Representations*.
- Chung, J.; Gulcehre, C.; Cho, K.; and Bengio, Y. 2014. Empirical evaluation of gated recurrent neural networks on sequence modeling. In *Advances in Neural Information Processing Systems Workshop*.
- Dai, Z.; Yang, Z.; Yang, Y.; Carbonell, J.; Le, Q. V.; and Salakhutdinov, R. 2019. Transformer-xl: Attentive language models beyond a fixed-length context. In *Proceedings of the Annual Meeting of the Association for Computational Linguistics*, 2978–2988.
- Geng, X.; Li, Y.; Wang, L.; Zhang, L.; Yang, Q.; Ye, J.; and Liu, Y. 2019. Spatiotemporal multi-graph convolution network for ride-hailing demand forecasting. In *Proceedings of the AAAI Conference on Artificial Intelligence*, 3656–3663.
- Guo, S.; Lin, Y.; Feng, N.; Song, C.; and Wan, H. 2019. Attention based spatial-temporal graph convolutional networks for traffic flow forecasting. In *Proceedings of the AAAI Conference on Artificial Intelligence*, 922–929.
- Guo, S.; Lin, Y.; Wan, H.; Li, X.; and Cong, G. 2021. Learning dynamics and heterogeneity of spatial-temporal graph data for traffic forecasting. *IEEE Transactions on Knowledge and Data Engineering*.
- Jeha, P.; Bohlke-Schneider, M.; Mercado, P.; Kapoor, S.; Nirwan, R. S.; Flunkert, V.; Gasthaus, J.; and Januschowski, T. 2022. PSA-GAN: progressive self attention GANs for synthetic time series. In *International Conference on Learning Representations*.
- Jiang, J.; Zhang, J.; and Zhang, K. 2020. Cascaded semantic and positional self-attention network for document classification. In *Conference on Empirical Methods in Natural Language Processing*, 669–677.
- Jiang, R.; Yin, D.; Wang, Z.; Wang, Y.; Deng, J.; Liu, H.; Cai, Z.; Deng, J.; Song, X.; and Shibasaki, R. 2021. DL-Traff: Survey and benchmark of deep learning models for urban traffic prediction. In *Proceedings of the ACM International Conference on Information & Knowledge Management*, 4515–4525.
- Jiang, W.; and Luo, J. 2021. Graph neural network for traffic forecasting: A Survey. *arXiv*.
- Kingma, D. P.; and Ba, J. 2015. Adam: A method for stochastic optimization. In *International Conference on Learning Representations*.
- Li, F.; Feng, J.; Yan, H.; Jin, G.; Jin, D.; and Li, Y. 2021. Dynamic graph convolutional recurrent network for traffic prediction: Benchmark and solution. *arXiv*.
- Li, M.; and Zhu, Z. 2021. Spatial-temporal fusion graph neural networks for traffic flow forecasting. In *Proceedings of the AAAI Conference on Artificial Intelligence*, 4189–4196.
- Li, Y.; Yu, R.; Shahabi, C.; and Liu, Y. 2018. Diffusion convolutional recurrent neural network: Data-driven traffic forecasting. In *International Conference on Learning Representations*.
- Ma, X.; Dai, Z.; He, Z.; Ma, J.; Wang, Y.; and Wang, Y. 2017. Learning traffic as images: A deep convolutional neural network for large-scale transportation network speed prediction. *Sensors*, 17(4): 818.
- Makhzani, A.; Shlens, J.; Jaitly, N.; and Goodfellow, I. 2016. Adversarial autoencoders. In *International Conference on Learning Representations*.
- Makridakis, S.; and Hibon, M. 1997. ARMA models and the Box–Jenkins methodology. *Journal of forecasting*, 16(3): 147–163.
- Raffel, C.; Shazeer, N.; Roberts, A.; Lee, K.; Narang, S.; Matena, M.; Zhou, Y.; Li, W.; and Liu, P. J. 2020. Exploring the limits of transfer learning with a unified text-to-text transformer. *Journal of Machine Learning Research*, 21(140): 1–67.
- Shaw, P.; Uszkoreit, J.; and Vaswani, A. 2018. Self-Attention with Relative Position Representations. In *Proceedings of the Conference of the North American Chapter of the Association for Computational Linguistics: Human Language Technologies*, 464–468.

SHI, X.; Chen, Z.; Wang, H.; Yeung, D.-Y.; Wong, W.-k.; and WOO, W.-c. 2015. Convolutional LSTM network: A machine learning approach for precipitation nowcasting. In *Advances in Neural Information Processing Systems*, 802–810.

Song, C.; Lin, Y.; Guo, S.; and Wan, H. 2020. Spatial-temporal synchronous graph convolutional networks: A new framework for spatial-temporal network data forecasting. In *Proceedings of the AAAI Conference on Artificial Intelligence*, 914–921.

Thomas N. Kipf, M. W. 2017. Semi-supervised classification with graph convolutional networks. In *International Conference on Learning Representations*.

Vaswani, A.; Shazeer, N.; Parmar, N.; Uszkoreit, J.; Jones, L.; Gomez, A. N.; Kaiser, Ł.; and Polosukhin, I. 2017. Attention is all you need. In *Advances in Neural Information Processing Systems*, 6000–6010.

Wu, C.-H.; Ho, J.-M.; and Lee, D.-T. 2004. Travel-time prediction with support vector regression. *IEEE Transactions on Intelligent Transportation Systems*, 5(4): 276–281.

Wu, S.; Xiao, X.; Ding, Q.; Zhao, P.; Wei, Y.; and Huang, J. 2020. Adversarial sparse transformer for time series forecasting. In *Advances in Neural Information Processing Systems*, 17105–17115.

Wu, Z.; Pan, S.; Chen, F.; Long, G.; Zhang, C.; and Yu, P. S. 2021. A comprehensive survey on graph neural networks. *IEEE Transactions on Neural Networks and Learning Systems*, 32(1): 4–24.

Wu, Z.; Pan, S.; Long, G.; Jiang, J.; and Zhang, C. 2019. Graph WaveNet for deep spatial-temporal graph modeling. In *Proceedings of the International Joint Conference on Artificial Intelligence*, 1907–1913.

Yoon, J.; Jarrett, D.; and van der Schaar, M. 2019. Time-series generative adversarial networks. In *Advances in Neural Information Processing Systems*, 5508–5518.

Yu, B.; Yin, H.; and Zhu, Z. 2018. Spatio-temporal graph convolutional networks: A deep learning framework for traffic forecasting. In *Proceedings of the International Joint Conference on Artificial Intelligence*, 3634–3640.

Yu, H.; Wu, Z.; Wang, S.; Wang, Y.; and Ma, X. 2017. Spatiotemporal recurrent convolutional networks for traffic prediction in transportation networks. *Sensors*, 17(7): 1501.

Zhang, J.; Zheng, Y.; Qi, D.; Li, R.; Yi, X.; and Li, T. 2018. Predicting citywide crowd flows using deep spatio-temporal residual networks. *Artificial Intelligence*, 259: 147–166.

Zhang, Y.; Wang, S.; Chen, B.; Cao, J.; and Huang, Z. 2021. TrafficGAN: Network-scale deep traffic prediction with generative adversarial nets. *IEEE Transactions on Intelligent Transportation Systems*, 22(1): 219–230.

Zheng, C.; Fan, X.; Wang, C.; and Qi, J. 2020. GMAN: A graph multi-attention network for traffic prediction. In *Proceedings of the AAAI Conference on Artificial Intelligence*, 1234–1241.

Zhou, T.; Ma, Z.; Wen, Q.; Wang, X.; Sun, L.; and Jin, R. 2022. FEDformer: Frequency enhanced decomposed transformer for long-term series forecasting. In *International Conference on Machine Learning*, 27268–27286.

Zivot, E.; and Wang, J. 2006. Vector autoregressive models for multivariate time series. *Modeling financial time series with S-PLUS*, 369–413.

Appendix

In this section, we provide implementation details, evaluation metrics, and supplemental experiments to reveal more interesting findings.

A Implementation Details

Our model stacks two layers of DAAGCN for capturing dynamic spatial-temporal dependencies from data automatically and maintaining the global properties and statistics of traffic series aligned with ground truth. Our model is based on GRU backbone to capture temporal correlations, thereby the hidden output at the last time step is utilized as the whole representation of the historical traffic series. Then, a linear transformation (MLP) is applied to map it to the traffic prediction for all horizons.

For all baselines, some of reported results are directly cited from existing works (Bai et al. 2020; Cao et al. 2020) while some of them are conducted by ourselves using authors provided source code under each model’s own optimal hyper-parameter setting, following original paper report. For reproducible checking, the hyper-parameters of DAAGCN are summarized in the following: We set the number of hidden units to 64 for all the GRU cells and the batch size to 64. Grid search is adopted to search the important weights of each information terms λ_1 , λ_2 , and λ_3 in Eq. 4 among $\{0, 1\}$, the trade-off weights of adversarial training α and β in Eq. 7 among $\{0.001, 0.01, 0.1, 1.0\}$, the embedding dimension among $\{1, 2, 3, 4, 5, 6, 7, 8, 9, 10, 12, 15\}$, and the learning rate among $\{0.0001, 0.0003, 0.001, 0.003, 0.005, 0.009\}$ for the all datasets. The performance results of different embedding dimensions over all datasets are shown in Table 5. Finally, the optimal hyper-parameters of DAAGCN is that $\lambda_1 = 1$, $\lambda_2 = 1$, and $\lambda_3 = 1$, $\alpha = 0.01$ and $\beta = 1.0$, the learning rate $\eta = 0.003$, and the embedding dimension d is set to 4 for PEMS03 dataset, 6 for PEMS04 dataset, 10 for PEMS07, and 4 for PEMS08 dataset.

Moreover, we optimize the model with the Adam (Kingma and Ba 2015) optimizer for 120 epochs to make sure the model be converged stably. However, we do not leverage weights decay and gradient normalization while employing learning rate decay with the decay rate of 0.3 at 80 and 100 epochs based on our model’s faster convergence to avoid gradient vibrating. Finally, we save the best model under the best performance in the validation set, and conduct traffic predictions with the best model.

B Evaluation Metrics

In this paper, we employ three commonly used metrics, i.e., Mean Absolute Error (MAE), Root Mean Square Error (RMSE), and Mean Absolute Percentage Error (MAPE), to evaluate our model performance. Specifically, let $\mathbf{X}^{(t)} \in \mathbb{R}^{N \times C}$ (in our work, we consider $C = 1$) and $\hat{\mathbf{X}}^{(t)} \in \mathbb{R}^{N \times C}$ be the ground truth traffic of all nodes and be the predicted traffic results at time step t , respectively. Ω is indices

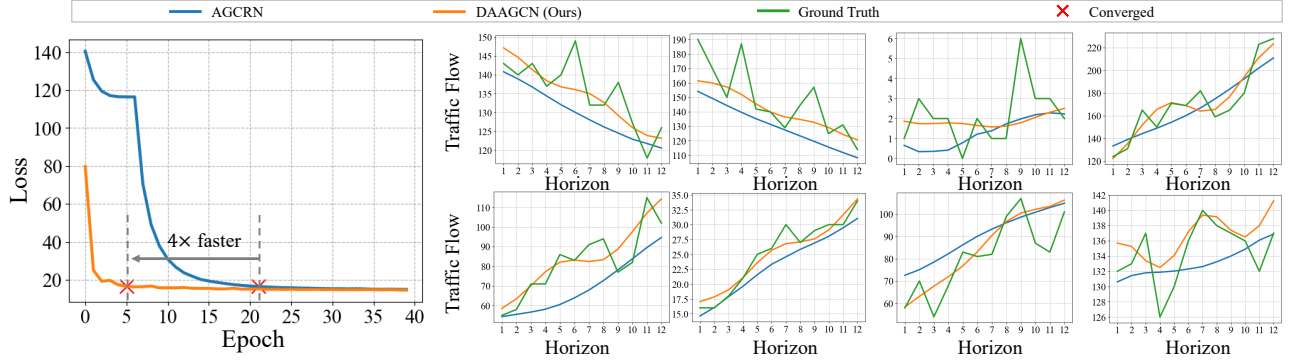


Figure 6: Convergence and predicted results of DAAGCN on PEMS03 dataset. The left sub-figure demonstrates that DAAGCN converges 4 times faster than AGCRN and yields lower training loss. The right eight sub-figures, corresponding to randomly selected eight nodes, show the predicted traffic flow at each horizon. It can be observed that the predicted results of DAAGCN are closer to ground truth and have a more similar global trend to ground truth.

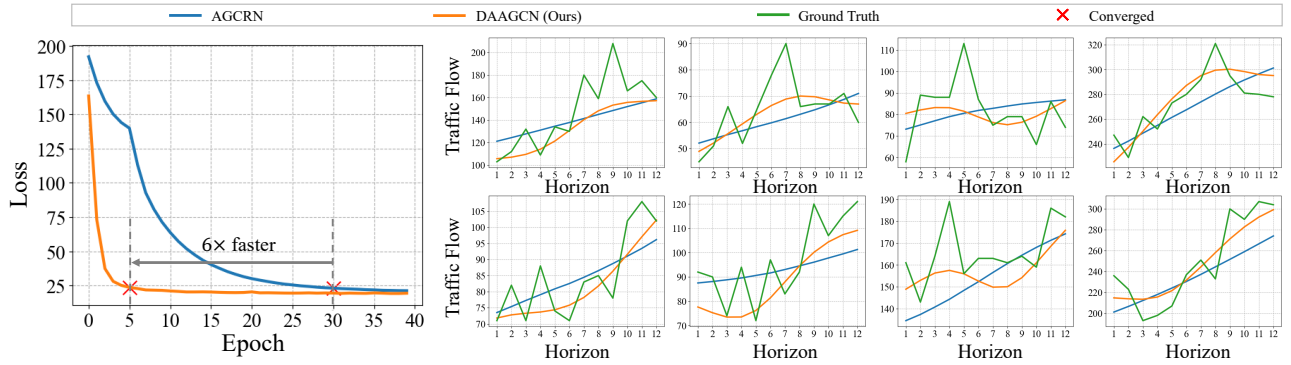


Figure 7: Convergence and predicted results of DAAGCN on PEMS04 dataset. The left sub-figure demonstrates that DAAGCN converges 6 times faster than AGCRN and yields lower training loss. The right eight sub-figures, corresponding to randomly selected eight nodes, show the predicted traffic flow at each horizon. It can be observed that the predicted results of DAAGCN are closer to ground truth and have a more similar global trend to ground truth.

of observed samples. The above three metrics are defined as follows:

- Mean Absolute Error (MAE)

$$\text{MAE} = \frac{1}{|\Omega|} \sum_{i \in \Omega} |\mathbf{X}^{(t)} - \hat{\mathbf{X}}^{(t)}| \quad (10)$$

- Root Mean Square Error (RMSE)

$$\text{RMSE} = \sqrt{\frac{1}{|\Omega|} \sum_{i \in \Omega} (\mathbf{X}^{(t)} - \hat{\mathbf{X}}^{(t)})^2} \quad (11)$$

- Mean Absolute Percentage Error (MAPE)

$$\text{MAPE} = \frac{1}{|\Omega|} \sum_{i \in \Omega} \left| \frac{\mathbf{X}^{(t)} - \hat{\mathbf{X}}^{(t)}}{\mathbf{X}^{(t)}} \right| \quad (12)$$

C Supplemental Experiments

C.1 Faster Model Convergence As shown on the left side of Fig. 2, 6, 7, and 8, our proposed DAAGCN enjoys up to 9 times faster model convergence, compared with the

state-of-the-art model AGCRN (Bai et al. 2020) that also employs adaptive graph generation. In addition, DAAGCN achieves the best prediction performance on all metrics on four benchmark datasets (see Table 1). These show that combining GCNs with GANs has great potential for traffic forecasting, i.e., faster convergence and better predicted results.

C.2 Multi-Step Prediction The traffic flow predictions at each horizon are shown on the right side of Fig. 2, 6, 7, and 8. We observe that the predicted results of DAAGCN are closer to ground truth, and DAAGCN models the dynamics of traffic series better than AGCRN, which might be because of the maintained consistency of the global properties and statistics of predicted time series.

Moreover, as shown in Fig. 9, we observe that DAAGCN consistently achieves lower prediction errors, i.e., MAE, RMSE, and MAPE, on all metrics for all horizons on PEMS08 dataset by a significant margin, compared with three representative the state-of-the-art spatial-temporal models. Our proposed DAAGCN demonstrates its superiority in short term and long term forecasting. In addition,

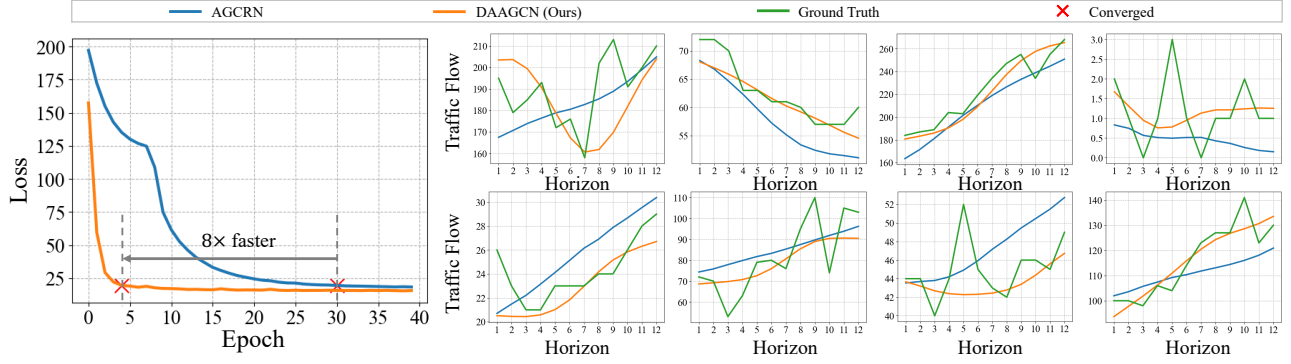


Figure 8: Convergence and predicted results of DAAGCN on PEMS08 dataset. The left sub-figure demonstrates that DAAGCN converges 8 times faster than AGCRN and yields lower training loss. The right eight sub-figures, corresponding to randomly selected eight nodes, show the predicted traffic flow at each horizon. It can be observed that the predicted results of DAAGCN are closer to ground truth and have a more similar global trend to ground truth.

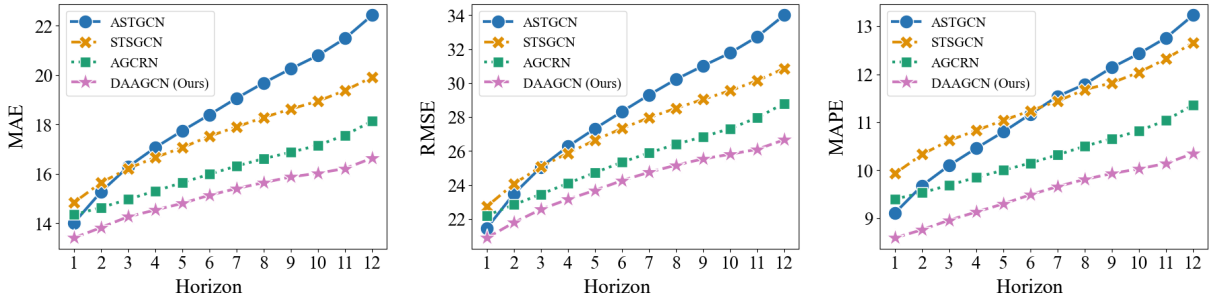


Figure 9: Prediction performance comparison at each horizon on PEMS08 dataset, in terms of MAE, RMSE, and MAPE.

the performance of all models gradually decreases as the horizon increases. Nevertheless, DAAGCN shows a much slower performance deterioration than the selected baseline models.

C.3 Hyperparameter Study In GCN-based models, the embedding dimension d of node embeddings and time-varying embeddings has a significant impact on model performance and the computational cost. The basic principle is that d should not be set too small (insufficient representation) and too large (over-fitting and time-consuming problem). Therefore, we further report the prediction performance of DAAGCN with different embedding dimension among $\{1, 2, 3, 4, 5, 6, 7, 8, 9, 10, 12, 15\}$ on PEMS03, PEMS04, PEMS07, and PEMS08 four traffic benchmark datasets, as shown in Table 5. We observe that the prediction performance of the model first increases to an optimal result and then decreases as the embedding dimension increases. Finally, the optimal embedding dimension d is 4 for PEMS03 dataset, 6 for PEMS04 dataset, 10 for PEMS07, and 4 for PEMS08 dataset.

C.4 More Graph Generation We analyze the influence of different coefficient weights λ when $\Delta_1 = +, \Delta_2 = +$, and further investigate the cases of multiplication ($\Delta_1 = \odot, \Delta_2 = \odot$), concatenation ($\Delta_1 = \parallel, \Delta_2 = \parallel$), and hybrid ($\Delta_1 = +, \Delta_2 = \odot$) fusion for the homologous term

and heterologous term in DAGG. Specifically, let E_{node}^i and E_{time}^t be the i th node embedding and time-varying embedding at time step t . Then, the multiplication A, concatenation B, and hybrid C and D fusion for homologous term and heterologous term can be formulated as:

$$\begin{aligned}
 A &= A_{ij} = \lambda^1 \{ E_{\text{node}}^i \parallel E_{\text{time}}^t, E_{\text{node}}^j \parallel E_{\text{time}}^t \} \\
 B &= A_{ij} = \lambda^2 \{ E_{\text{node}}^i \odot E_{\text{time}}^t, E_{\text{node}}^j \odot E_{\text{time}}^t \} \\
 C &= A_{ij} = \lambda^3 \{ E_{\text{node}}^i + E_{\text{time}}^t, E_{\text{node}}^j \odot E_{\text{time}}^t \} \\
 D &= A_{ij} = \lambda^4 \{ E_{\text{node}}^i \odot E_{\text{time}}^t, E_{\text{node}}^j + E_{\text{time}}^t \}
 \end{aligned} \tag{13}$$

where

$$\lambda^1 = \lambda^2 = \lambda^3 = \lambda^4 = 1 \tag{14}$$

The experimental results on PEMS04 and PEMS08 datasets are shown in Table 6. We derive the following interesting findings: 1) the equally fusing homologous term and heterologous term in Eq. 13 achieves optimal performance on both datasets, indicating the same importance of each information term when $\Delta_1 = +, \Delta_2 = +$; 2) hybrid fusion seems a promising way to combine each information terms. In some cases, they even achieve the best performance, e.g., **12.23** on MAPE on PEMS04 dataset, and **14.98** on MAE on PEMS08 dataset.

Table 5: Influence of different dimensions of node and time-varying embeddings on four datasets. Bold scores are the best in each column.

# Embs. Dim.	PEMS03			PEMS04		
	MAE	RMSE	MAPE(%)	MAE	RMSE	MAPE(%)
1	16.74	27.49	19.03	22.87	36.16	15.24
2	16.33	27.17	16.46	22.24	35.24	14.96
3	14.92	25.47	14.48	19.38	31.23	12.87
4	14.77	25.66	13.92	19.15	31.08	12.53
5	14.86	25.86	14.91	19.03	31.20	12.46
6	14.81	25.99	14.30	18.81	30.68	12.25
7	14.97	26.53	14.34	18.93	31.42	12.37
8	14.81	26.30	14.42	19.00	31.62	12.40
9	15.00	26.34	14.94	18.98	31.58	12.44
10	15.02	26.37	14.87	18.84	31.29	12.25
12	15.01	26.27	14.48	19.00	31.62	12.40
15	15.00	26.62	14.67	18.99	31.60	12.54
# Embs. Dim.	PEMS07			PEMS08		
	MAE	RMSE	MAPE(%)	MAE	RMSE	MAPE(%)
1	25.65	40.79	12.72	17.44	27.45	12.54
2	25.03	40.68	11.25	17.08	27.08	11.72
3	22.36	36.27	9.81	15.24	24.15	9.97
4	21.23	35.40	8.98	15.15	24.26	9.51
5	21.18	35.29	8.84	15.15	24.42	9.56
6	20.96	35.17	8.95	15.33	24.68	9.63
7	21.07	35.96	8.77	15.37	24.61	9.74
8	20.80	35.19	8.75	15.33	24.65	9.75
9	20.77	35.04	8.82	15.57	24.84	9.90
10	20.70	35.16	8.57	15.19	24.78	9.58
12	20.47	34.99	8.61	15.52	25.01	9.77
15	20.58	35.12	8.72	15.36	24.70	9.98

C.5 Activation Function For graph generation, many previous works (Wu et al. 2019; Bai et al. 2020; Chen et al. 2020; Guo et al. 2019) generally employ RELU with SOFTMAX as non-linear activation function by default.

However, there is rarely an in-depth study to discuss which activation function can achieve the best performance and where it should be used.

Therefore, we present a comprehensive study to discuss the influence of activation function on graph generation. We explore commonly used seven activation functions, including RELU, LEAKRELU, ELU, TANH, SIGMOID, SWISH, and SOFTMAX. The visualization of activation functions are shown in Fig. 10 and the formulations are listed in Eq. 14-20. We consider two aspects of using activation functions to generate adaptive adjacency matrices (graph): 1) directly applying different activation functions on the adaptive adjacency matrices, formulated as $A = \sigma(\cdot)$; 2) based on 1), further applying softmax to normalize value. The experimental results are shown in Table 7. To enhance interpretability, adaptive adjacency matrices at the last time step with different activation functions are visualized in Fig. 11, including the cases of (1) and (2). Note that all figures are visualized before any activation function, as it represents a more real-

istic correlation in the traffic system. Based on Table 7, Fig. 11, and Fig. 12, we derive the following observations:

- The last column in each case (i.e., (1) and (2)) obtains the optimal performance, i.e., $A = \text{softmax}(\cdot)$. Compared with other adaptive adjacency matrices, (h) seems more sparse, which is consistent with many existing works (Li et al. 2018; Yu, Yin, and Zhu 2018; Thomas N. Kipf 2017; Zhou et al. 2022).
- For aspect 1), all results except the last *softmax* case are much worse than all cases in aspect 2). It implies that normalized value using *softmax* is necessary to avoid large value resulting in gradient vanishing or exploration problem and further harms model performance in magnitude.
- For aspect 2), different activation functions achieve similar performance on all metrics. In particular, the last *none* case, i.e., $A = \text{softmax}(\cdot)$, consistently gets the best performance while *ReLU* achieves fairly close performance. In our work, we use $A = \text{softmax}(\cdot)$ by default.
- Another interesting finding is that distance adjacency matrix is much sparser than any cases of adaptive ad-

Table 6: Influence of different coefficient weights for the homologous term and heterologous term in DAGG on PEMS04 and PEMS08 datasets (full experiment). Bold scores are the best in each row.

Results	PEMS04									
	$\lambda = (\lambda_1, \lambda_2, \lambda_3)$						A	B	C	D
	(1,0,0)	(1,1,0)	(0,1,1)	(1,0,1)	(0,1,0)	(1,1,1)				
MAE	19.22	19.12	18.98	18.98	18.96	18.81	19.11	18.88	18.95	18.85
RMSE	32.12	31.92	31.66	31.71	31.53	30.68	31.98	31.05	31.39	31.20
MAPE(%)	12.48	12.46	12.51	12.50	12.32	12.25	12.53	12.26	12.23	12.24
Results	PEMS08									
	$\lambda = (\lambda_1, \lambda_2, \lambda_3)$						A	B	C	D
	(1,0,0)	(1,1,0)	(0,1,1)	(1,0,1)	(0,1,0)	(1,1,1)				
MAE	15.31	15.65	15.45	15.34	15.54	15.15	15.21	14.98	15.23	15.10
RMSE	24.65	25.35	24.82	24.88	25.27	24.26	24.60	24.42	24.86	24.63
MAPE(%)	9.77	10.18	9.99	9.88	9.81	9.51	9.74	9.66	9.58	9.62

Table 7: Influence of different activation functions for dynamic adaptive adjacency matrix (graph) generation under two aspects. Bold scores are the best in each row.

Results	$A = \sigma(\cdot)$						
	ReLU	LEAKReLU	ELU	TANH	SIGMOID	SWISH	SOFTMAX
MAE	92.20	90.82	77.02	45.60	42.66	77.19	18.81
RMSE	126.15	125.95	108.19	67.24	64.56	109.55	30.68
MAPE(%)	78.05	71.13	70.84	37.74	31.51	75.02	12.25
Results	$A = \text{SOFTMAX}(\sigma(\cdot))$						
	ReLU	LEAKReLU	ELU	TANH	SIGMOID	SWISH	NONE
MAE	18.98	19.12	18.88	18.98	19.03	19.01	18.81
RMSE	31.76	32.07	31.33	31.59	31.64	31.74	30.68
MAPE(%)	12.30	12.38	12.27	12.35	12.35	12.46	12.25

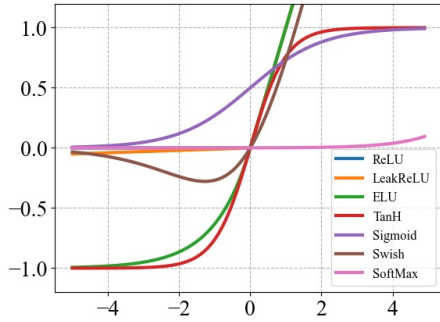


Figure 10: Visualization of activation functions.

jacency matrices (b)-(n). It indicates that too much compact representation of spatial-temporal dependencies between all nodes would cause too much information to be lost and is narrow to model complex and dynamical spatial-temporal dependencies in traffic systems.

The above seven activation functions are formulated as follows:

- ReLU

$$f(x) = \max(0, x) \quad (15)$$

- LeakReLU

$$f(x) = \max(\alpha x, x) \quad (16)$$

- ELU

$$f(x) = \begin{cases} x, & \text{if } x > 0 \\ \alpha(e^x - 1), & \text{if } x \leq 0 \end{cases} \quad (17)$$

- TanH

$$f(x) = \frac{e^x - e^{-x}}{e^x + e^{-x}} = \frac{2}{1 + e^{-2x}} - 1 \quad (18)$$

- Sigmoid

$$f(x) = \frac{1}{1 + e^{-x}} \quad (19)$$

- Swish

$$f(x) = \frac{x}{1 + e^{-x}} \quad (20)$$

- SoftMax

$$f(x)_i = \frac{e^{x_i}}{\sum_{j=1}^K e^{x_j}} \quad \text{for } i = 1, 2, \dots, K \quad (21)$$

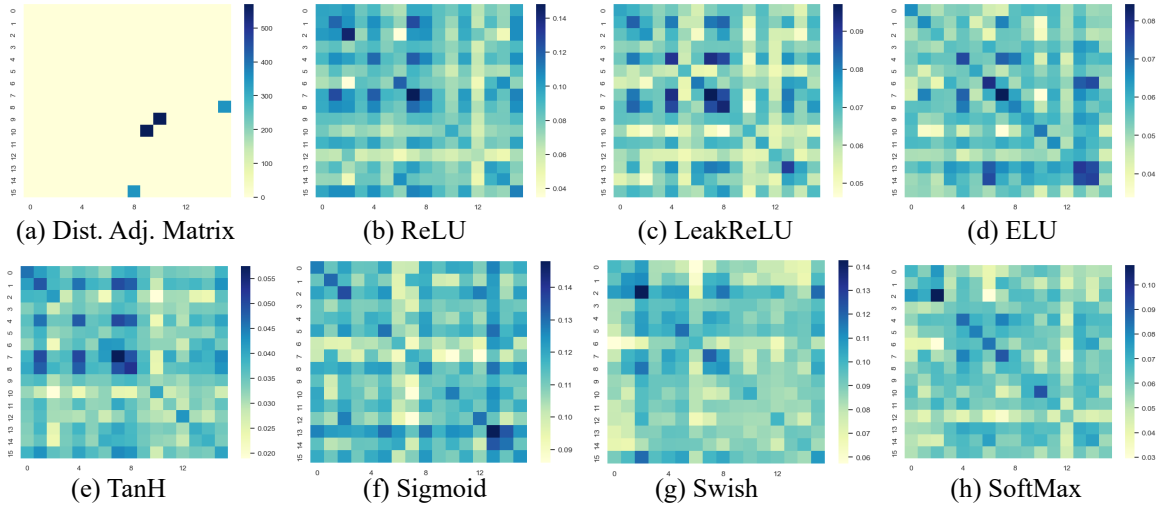


Figure 11: Visualization of learned adaptive adjacency matrices (graph) at the last time step with different activation functions, corresponding to the top part of Table 7. (a) is the distance adjacency matrix. (b)-(h) are the adaptive adjacency matrices obtained by applying different activation functions directly, formulated as $A = \sigma(\cdot)$.

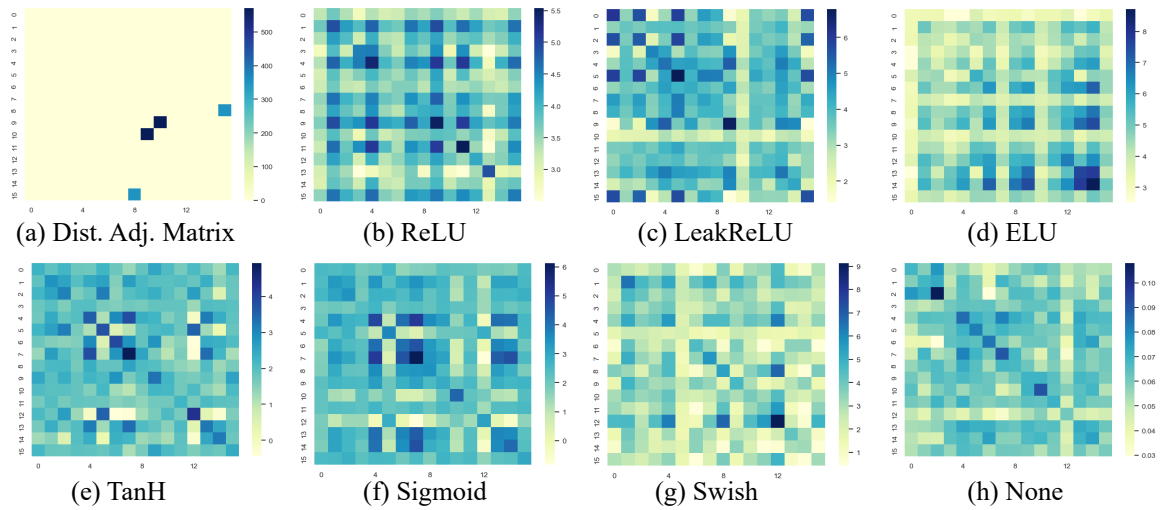


Figure 12: Visualization of learned adaptive adjacency matrices (graph) at the last time step with different activation functions, corresponding to the bottom part of Table 7. (a) is the distance adjacency matrix. (b)-(h) are the adaptive adjacency matrices obtained by applying softmax on different activation functions, formulated as $A = \text{softmax}(\sigma(\cdot))$.